# Prediction of quasi-static crack onset and growth in laminated composites using Acoustic Emission technique

Milad Saeedifar[*], Mohamad Fotouhi[*], Mehdi Ahmadi najafabadi[*1], Hossein Hosseini Toudeshky[**]

[*]*Non-destructive Testing Lab, Department of Mechanical Engineering, Amirkabir University of Technology, Tehran, Iran*
[**]*Department of Aerospace Engineering, Amirkabir University of Technology, Tehran, Iran*

## Abstract

Delamination is the most common mode of failure mechanism in laminated composites. It leads to loss of structural strength and stiffness. In this paper, mode I delamination is investigated using mechanical data and Acoustic Emission (AE) signals. The main objective is to determine position of the crack tip during initiation and propagation of delamination and to evaluate interlaminar fracture toughness ($G_{IC}$) in the glass/epoxy composite specimens. Position of the crack tip during propagation of delamination in the specimens is identified using two methods. In the first method, by determining the velocity of the AE waves in the specimens and some filtration methods which are applied on the AE signals, position of the crack tip is determined at any time of the test. In the second method, the position of the crack tip is identified using cumulative energy of the AE signals. The relationship between cumulative AE energy and crack growth is developed and presented based on experimental data. Agreement between the predicted crack length and actual crack length verifies the presented procedures. Interlaminar fracture toughness of the specimens is also determined using three methods: a) ASTM standard methods, b) AE method and c) sentry function method, that combination of AE and mechanical informations. The sentry function method is a capable method for prediction of delamination trends. The results show that the AE method and sentry function method could represent the lower bound of the $G_{IC}$ values. These values are in a close agreement with the results of non-linearity methods which is recommended by ASTM standards and are more reproducible than ASTM results. Finally, the study indicates that AE method may be more suitable than conventional visual

[1]. Corresponding author; Tel: (+98 21) 6454 3431; Fax: +98 21 8871 2838; Email address: ahmadin@aut.ac.ir

methods for detection of crack tip position and to determine interlaminar fracture toughness in laminated composites.

**Keywords**: Delamination, Acoustic Emission, Sentry Function, Interlaminar Fracture Toughness

# 1. Introduction

The increased use of Glass Fiber Reinforced Plastics (GFRP) in many mechanical structures has resulted in a growing need for nondestructive-testing techniques for the monitoring of structural integrity. Delamination in GFRP has been a subject of intensive research for many years. This failure can be caused by improper manufacturing, the stresses between the layers of the composite and impact. Its effect on the structure may include a dramatic loss of residual strength and stiffness of GFRP [1].

Acoustic emission is a relatively new and rapidly growing active nondestructive-testing method that possesses some abilities which improve the reliability and confidence of delamination detection method [2-5]. This technique seems to be an appropriate tool to detect in-situ information about the damages that occur during initiation and propagation of delamination [6-8].

Determination of crack growth in structures has a vital role in the fracture mechanics and damage tolerance analyses [9]. AE have been utilized by some researchers to study the crack growth in homogeneous metallic materials such as Aluminum and Steel [10-15]. Yu et al. [16, 17] investigated crack growth in the ASTM A572 Grade 50 specimens using AE method. Energy of AE signals utilized for estimation of crack growth in the specimens. The results obtained from AE method have a good agreement with results of standard methods. They have shown that it is possible to acoustically detect growing cracks by continuous AE monitoring when certain precautions are taken with a properly designed instrumentation system

One of the most common damage mechanisms in the laminated composites is delamination. The onset and growth of delamination under different loading conditions is particularly troublesome in high-performance composite structures. Composite materials are the combination of two or more elements. Therefore the investigations of crack onset and growth by AE method have been lacking in literature,

primarily because of difficulties in eliminating extraneous background noise and separation of AE signals obtained from different damage sources. There are some studies about to investigate the delamination damage in composite materials by use of AE. Romhany et al. [18] offered the localization algorithm based on AE signals to predicted of delamination growth in the carbon/epoxy specimens under mode I loading condition. The results show that AE method capables predicted growth of the delamination during the tests. Paget [19] utilized the AE method to localization and identification of damage mechanisms that occurred in the carbon/epoxy plate under compression loading. Refahi et al. [20] study delamination in glass/polyester composites under mode I loading condition using AE. They determine the initiation of delamination and interlaminar fracture toughness of the specimens. Arumugam et al. [21] investigate delamination and the damage mechanisms in glass/epoxy composite specimens under mode I loading using AE and Fast Fourier Transform (FFT) analysis. They could distinguished fiber breakage and matrix cracking damage mechanisms. Matrix cracking induced AE signals with low amplitude and energy and fiber breakage made AE signals with high amplitude and energy. Silversides et al. [22] determined interlaminar fracture toughness of the carbon/epoxy composites under mode I, mode II and mixed-mode I & II loading condition by AE method.

The main purpose of the present investigation is to further explore the delamination onset and growth characteristics by acoustic emission method. At first, propagation of delamination is investigated by AE method. In order to predict the delamination length during the tests two methods offered: a) localization of AE signal sources method and b) cumulative AE energy method. Then, some new procedures based on AE are presented for the evaluation of interlaminar fracture toughness of the specimens. Finally, the study indicates that AE method may be more suitable than conventional visual methods for detection of crack tip position and to determine interlaminar fracture toughness in laminated composites.

# Experimental Procedures

## *1.1 Materials and specimens preparation*

The experimental work was carried out on the epoxy resin reinforced by the E-glass unidirectional and woven fibers with the density of 1.17 g/cm$^3$, 390 g/m$^2$ and 300 g/m$^2$, respectively. The laminates were prepared by hand lay-up. The starter crack was formed by inserting a Teflon film with a thickness of 20 μm at mid-plane during molding as an initial crack for delamination. The laminated composite test specimens consist of a rectangular shape and uniform thickness consists of 14 plies. Characteristics of the specimens used for this study are illustrated in Figure 1 and Table 1.

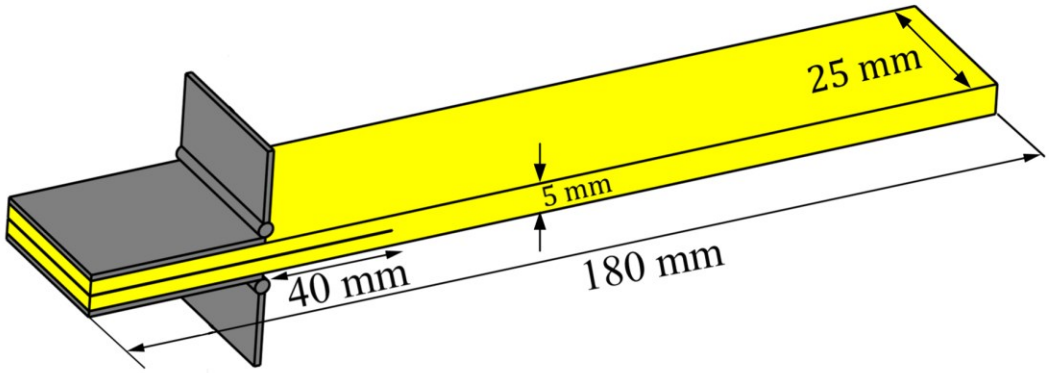


**Fig. 1** Specimens geometry and dimensions

**Table 1** Specification of the specimens

| Specimen names | Lay-up |
|---|---|
| **U** | Unidirectional [0] |
| **W** | Woven [0-90] |

## *1.2 Test procedure*

The tests done according to ASTM D5528 standard [23]. DCB test apparatus shown in Fig. 2 were used to apply load on the specimens. In DCB setup, an upward force is applied to split end of the laminate to create mode I. Delamination tests were carried out at a temperature of 24°C and at a constant displacement rate of 3 mm/min. The load and displacement were continuously measured and the crack length was recorded using a digital video camera (SONY HDR-XR150) with 25X optical zoom and 300X digital zoom. In order to investigate repeatability of the results, three samples were tested for each condition.

**Fig. 2** Experimental setup for specimens loading and the AE apparatus

## *1.3 Testing machine*

A properly calibrated tensile test machine (HIWA) in the range from 0.5 to 500 mm/min was used in a displacement control mode with a constant displacement. All the specimens were loaded with constant 3 mm/min crosshead rate.

### 1.4 AE device

AE events were recorded by using Acoustic Emission software AEWin and a data acquisition system Physical Acoustics Corporation (PAC) PCI-2 with a maximum sampling rate of 40 MHz. PICO which is a broadband, resonant-type, single-crystal piezoelectric transducer from PAC, was used as the AE sensor. The sensor has a resonance frequency of 513.28 kHz and an optimum operating range of 100–750 kHz. In order to provide good acoustic coupling between the specimen and the sensor, the surface of the sensor was covered with grease. The signal was detected by the sensor and enhanced by a 2/4/6-AST preamplifier. The gain selector of the preamplifier was set to 37 dB. The test sampling rate was 1 MHz with 16 bits of resolution between 10 and 100 dB.

# 2. Fracture Toughness

### 2.1 Energy release rate

In a body with linear elastic behavior, strain energy release rate (G) is expressed by Eq 1:

$$G = -\frac{dU}{Bda} \quad \text{(Eq 1)}$$

Where a, B and U are crack length, width and total elastic strain energy of the test specimens, respectively [24].

Energy release rate for mode I (DCB) test is as follow [23]:

$$G_I = \frac{3P\delta}{2B(a+|\Delta|)} \quad \text{(Eq 2)}$$

Where P, δ, B, a and Δ are the load, displacement of the load point, width of specimens, delamination length and crack length correction factor, respectively.

# 3. Results and discussion

## *3.1 Mechanical observation*

Delamination is the principal mode of failure in laminated composites that can be occurred under different loading modes, i.e. mode I, mode II and mode III. Through the different loading modes, mode I is the most common mode that occurred in the structures. This is due to lower energy which is required for the initiation of mode I delamination [25-27]. In order to investigate delamination in glass/ epoxy composites under mode I loading, the DCB specimens are loaded according to procedures represented in ASTM D5528.

Figure 3 shows load-displacement curve for specimen W. The diagram can be divided into three regions: I) from the beginning to the nonlinearity point of the curve, II) from the nonlinearity point to the maximum load and III) from the maximum load to end of the test. In the first region, load-displacement relation is linear. In this region, by increasing load the stored strain energy in the specimens is accumulated, but it doesn't reach to the critical value which is required for initiation of delamination. Therefore, the delamination does not onset [23]. In region (II), the slope of the load-displacement diagram decreases. At the beginning of this region, the stored strain energy in the specimens reaches to the critical value and delamination initiates [23]. In region (III), the delamination propagates and load carrier capacity of the specimen is reduced. Figures 4 and 5 show load-displacement and crack growth- displacement diagrams for specimens U and W. As can be seen from Figure 4, in specimen U, by increasing load up to 55 N, strain energy is accumulated in the specimen. When load reaches to 55 N, stored strain energy in the specimen (G) reaches to the critical value ($G_C$) and delamination initiates. Initial growth of the delamination is affected by fiber bridging phenomenon that occurred behind the crack tip and resists against crack growth. Due to this factor, after initial growth of the delamination, it is arrested and load increases to the maximum point that the bridged fibers are ruptured and delamination propagates. At the crack propagation region of the diagram, the load fall and jump correspond to crack propagation process which is affected by two following stages. Arresting stage: when the crack is arrested and the stored strain energy in the specimens increases. At

this stage the fiber bridging resistance is present and the crack growth rate is slow. Sudden extension and a consequent stop stage: At this stage bridged fibers are broken and the crack propagates instantaneously. After this sudden drop there is a consequent stop in the crack growth. Crack growth diagram shows run-arrest behavior for the specimen U. According to Figure 5, crack growth behavior in specimen W is stable state compared with specimen U. This is because of lower occurrence of the fiber bridging phenomenon in specimen W compared with specimen U.

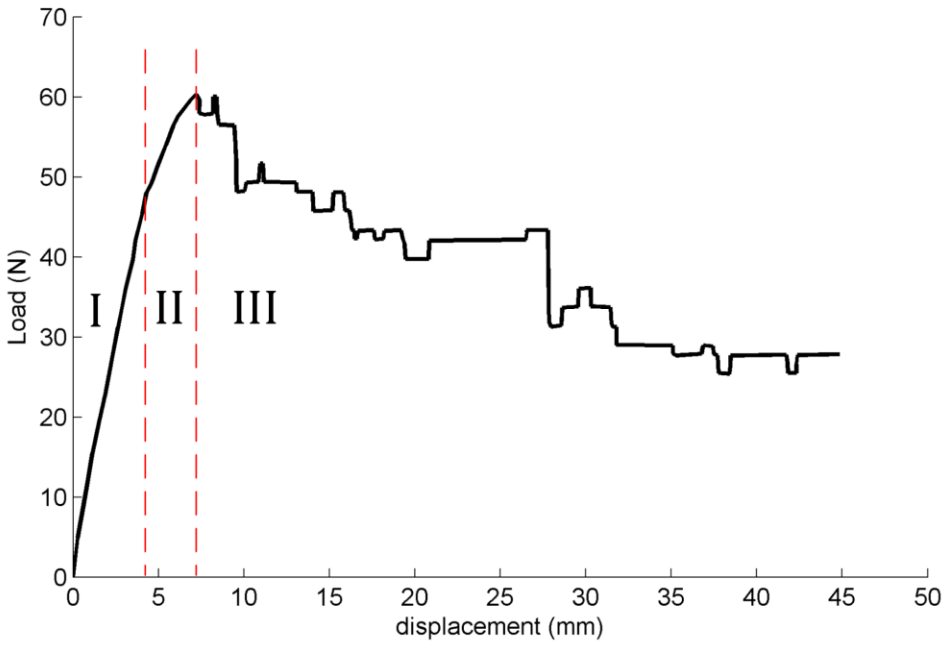


**Fig. 3** Three regions of the load-displacement diagram for specimen W

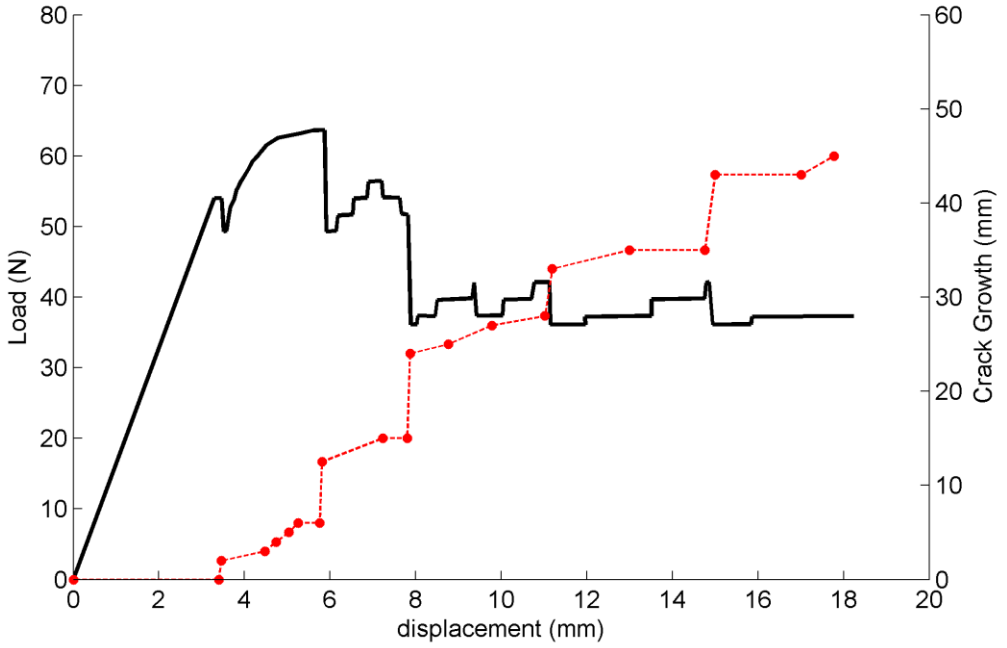


**Fig. 4** Load-displacement and crack length-displacement diagrams for specimen U

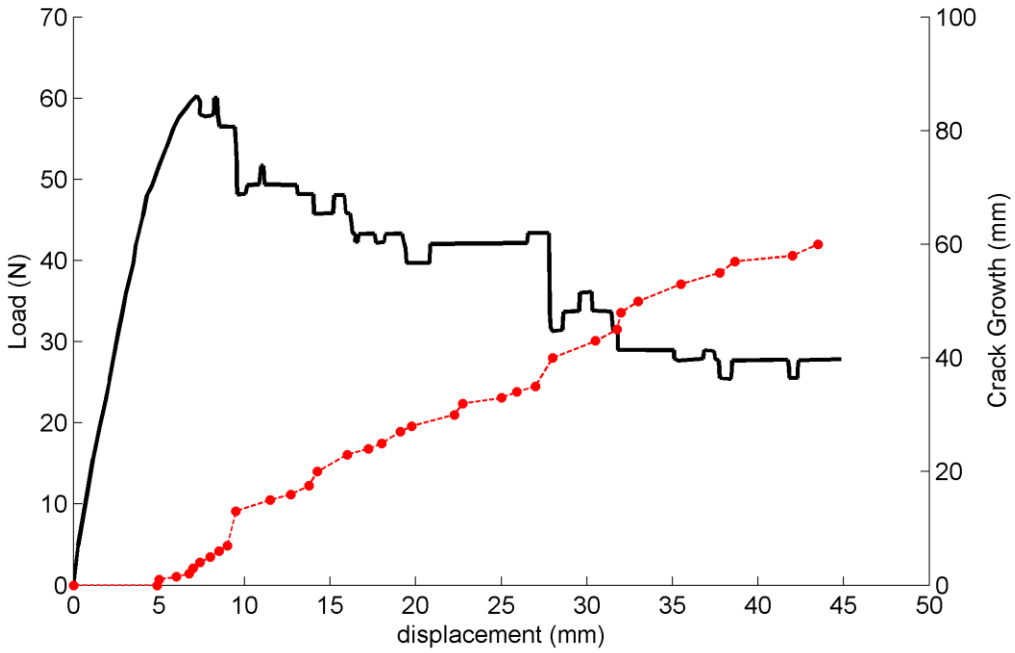


**Fig. 5** Load-displacement and crack length-displacement diagrams for specimen W

## 3.2 Crack Tip Localization

AE technique has high sensitivity and demonstrated reliability in detection of active cracks. A notable advantage of the AE technique is the capability of locating active cracks in the region where a crack is likely to occur [19, 28-29]. Detecting cracking signals is a necessary step in the application of AE techniques, because of, in addition to cracking signals, AE sensors are also sensitive to environmental noises. In this section, crack tip position in the specimens during the test is determined using two methods: 1) Crack tip localization using determining sources location of the AE signals, and 2) Crack tip localization using cumulative AE energy.

### *3.2.1 Crack tip localization using determining sources location of the AE signals*

In this method, in order to determine crack tip position, at first, AE wave velocity in the specimens must be specified. Velocity of the AE waves in the specimens was evaluated using standard pencil lead breakage test. In the pencil lead breakage test, two sensors are placed in the specific distances on the specimens. Then, pencil lead is broken on the surface of the specimen at a side of one of the sensors. The generated wave is detected by closer sensor and after a time delay the farther sensor senses the wave. By knowing the distance and time difference between two sensors, the AE wave velocity in the specimens is determined. For investigating of reproducibility, the test was repeated three times for the specimens. Also, to evaluate dependency of wave velocity to the delamination propagation and bending of arms of the specimens, these procedures are repeated three times during the crack propagation for the specimens. Figure 6 shows schematic of the pencil lead breakage tests. Table 2 represented the results of AE wave velocity in the specimens.

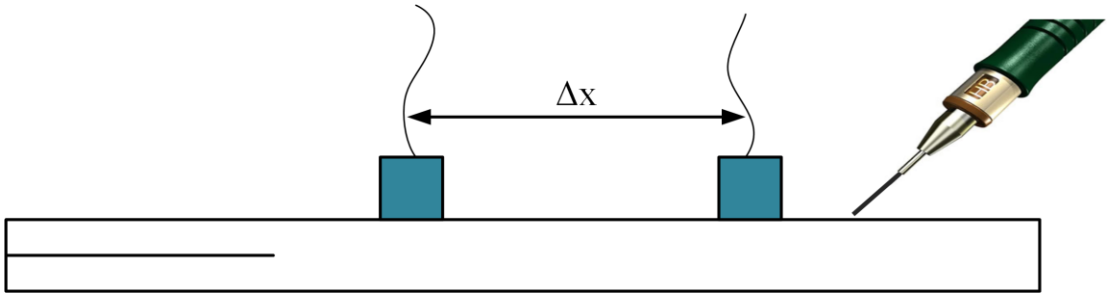


**Fig. 6** Schematic of pencil lead breakage test

**Table 2** AE wave velocity in the specimens

| Specimen | AE wave velocity (m/s) (Δa=0 mm) | AE wave velocity (m/s) (Δa=20 mm) | AE wave velocity (m/s) (Δa=40 mm) |
|---|---|---|---|
| **U** | 4668±1% | 4373±2% | 4274±2% |
| **W** | 3380±0.5% | 3220±1% | 3089±0.8% |

By loading the specimens and initiation of delamination growth, the AE signals are generated in the specimens. The generated AE signals are recorded using two sensors. The first sensor was located at 15 mm before the pre-delamination tip and the second located at 80 mm after the pre-delamination tip. By this procedures and post processing activities, AE noise signals that originated from out of the region between two sensors, such as environments, tensile machine, friction between hinges and grips and etc., are eliminated. After the tests, post processing activities are done. As a filtering action AE signals with zero energy and they which have rise time greater than duration, eliminated. Then, the AE signals that recorded by both sensors and are applied in the condition of Equation 3 are specified. According to the results of Table 2 and by knowing the arrival time difference between two sensors for each event, the location of the event is evaluated using Equation 3 (Figure 7).

$$\begin{cases} x_1 + x_2 = 95 \\ |x_2 - x_1| = C.(t_2 - t_1) \end{cases} \quad ; \quad \Delta t < \frac{95}{C} \qquad \text{(Eq. 3)}$$

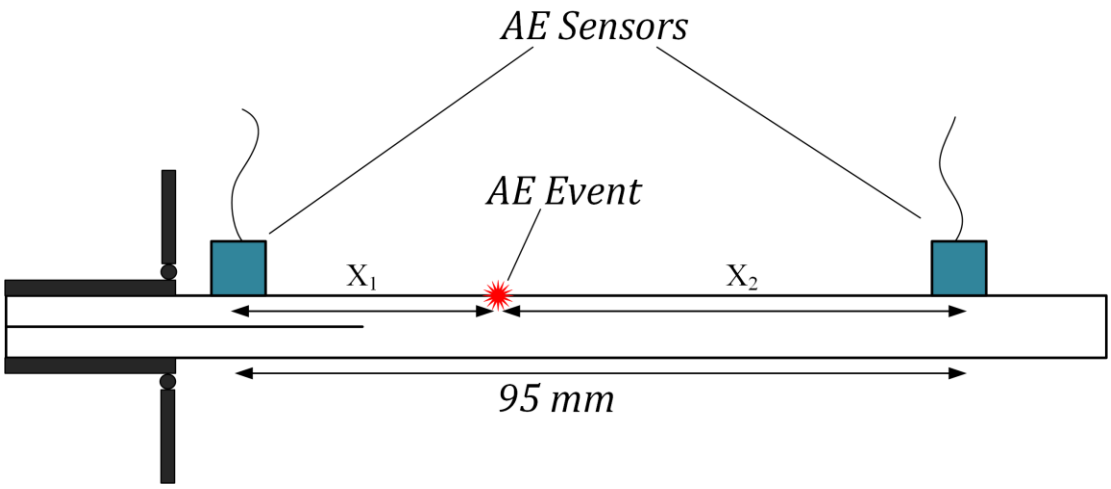


**Fig. 7** AE event localization procedures

Figure 8 shows predicted crack tip position that obtained from the proposed method for the specimen W V.S visually-detected crack tip position. As it is clear, the general trend of the AE results is in accordance with visual results, but, the bandwidth of the AE results is broadband.

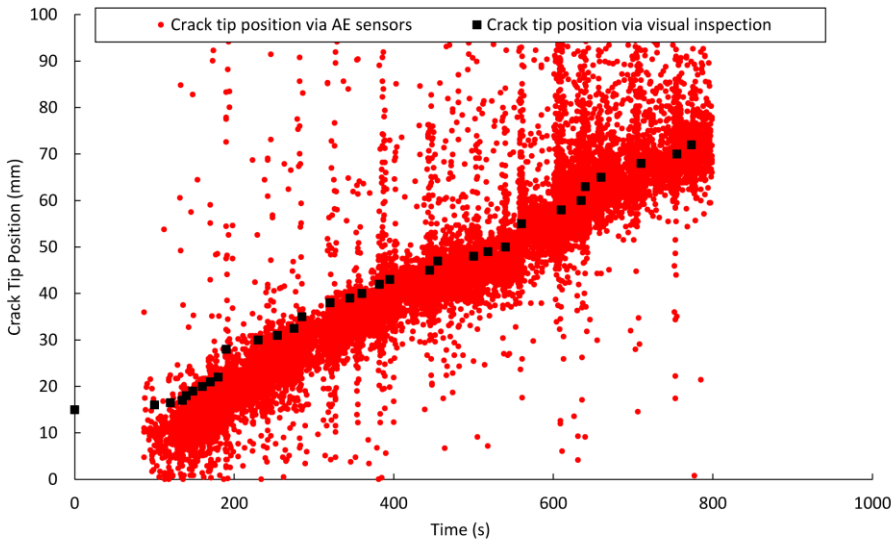


**Fig. 8** Predicted and actual crack tip position for specimen W

In order to reduce the bandwidth of the AE results, the following method is used. According to previous studies [], during delamination propagation in the composites, different damage mechanisms such as matrix cracking, fiber breakage and fiber-matrix debonding occur. These failure mechanisms

have a specific AE feature ranges such as amplitude, frequency and energy. Fiber breakage occurs due to failure of the bridged fibers in the small area behind the crack tip. Figure 9 shows the fiber bridging and fiber breakage phenomenon. Because of fiber breakage occurs near the crack tip region, by determining features of AE signals related to fiber breakage, other signals that can be originated from anywhere else on the specimen could be eliminated. In order to extract AE features of the fiber breakage signals and to create AE reference patterns, fiber tensile test is carried out. The fiber breakage test is done in a tension test on a bundle of about 1400±50 filaments (see Figure 10). Figure 11 shows amplitude and frequency ranges of fiber breakage.

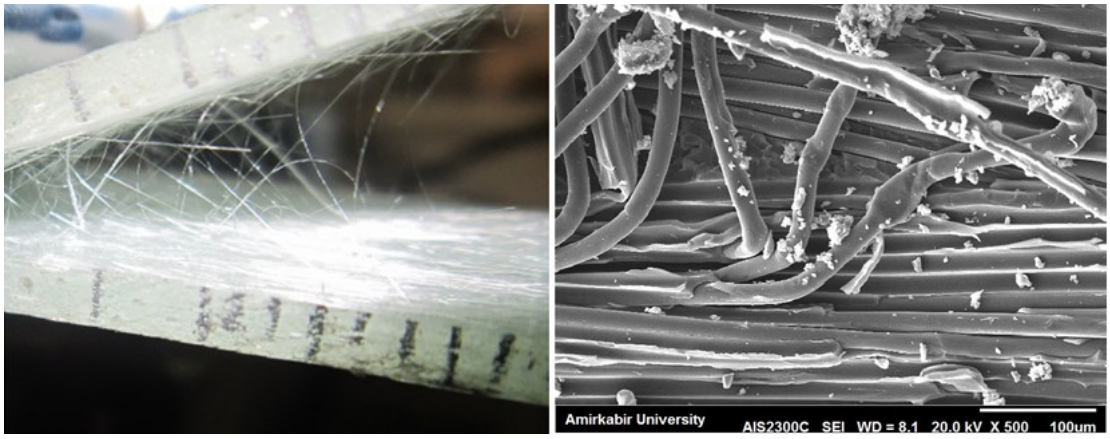


**Fig. 9** Fiber bridging and fiber breakage phenomeneon

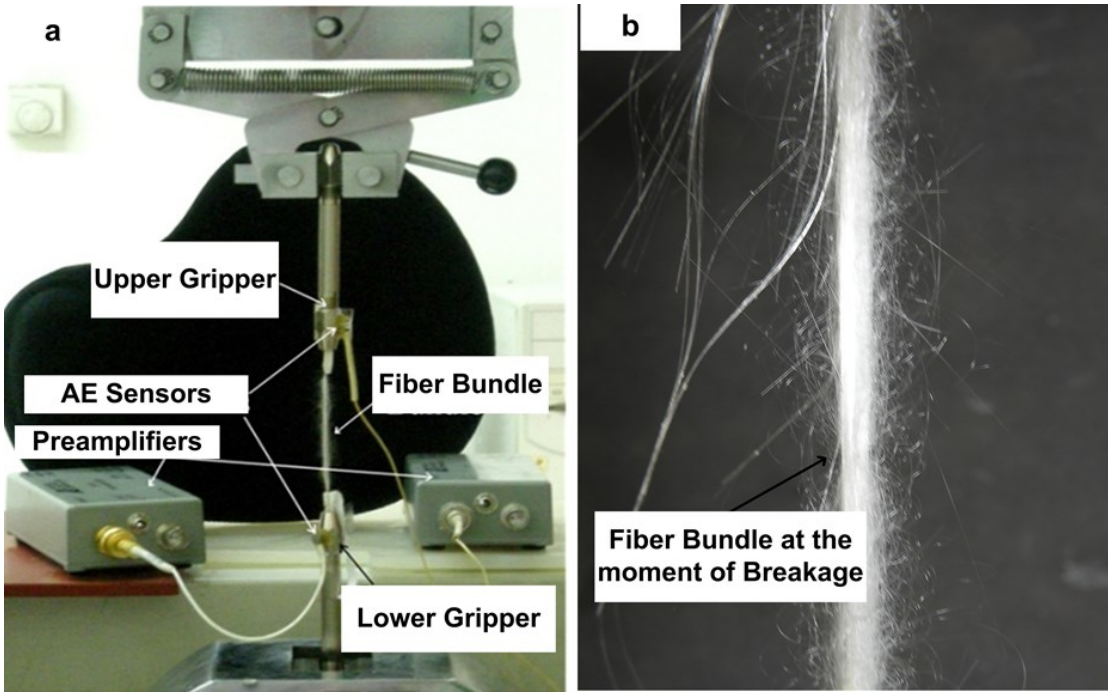


**Fig. 10** Fiber breakage test apparatus

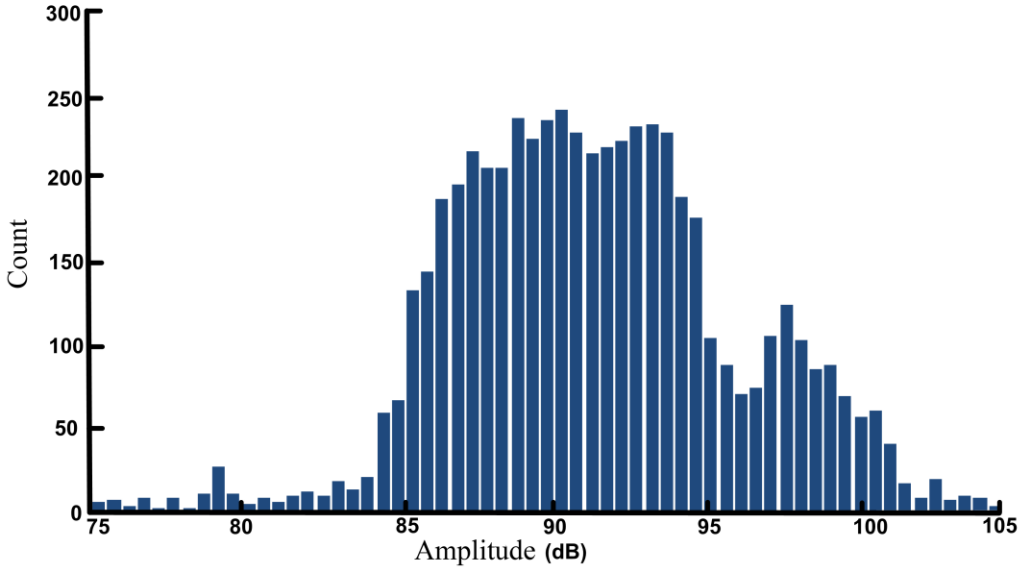


**Fig. 11** Amplitude distribution of the fiber breakage

In order to reduce the bandwidth of the AE data in Figure 8, AE signals which have amplitude lower than 85 dB or greater than 100 dB, are eliminated. Using this method, the bandwidth of the AE results

is reduced considerably (Figure 12.a). Taking the average of the signals that are generated at a time, leads to Figure 12.b. By elimination of events which have diversity greater than three time of the standard deviation from average line, the final crack tip position determined (Figure 12.c). As it is mentioned above, since the fiber bridging and fiber breakage occurred behind the delamination tip, thus, the upper bound of the represented events show the crack tip of the delamination.

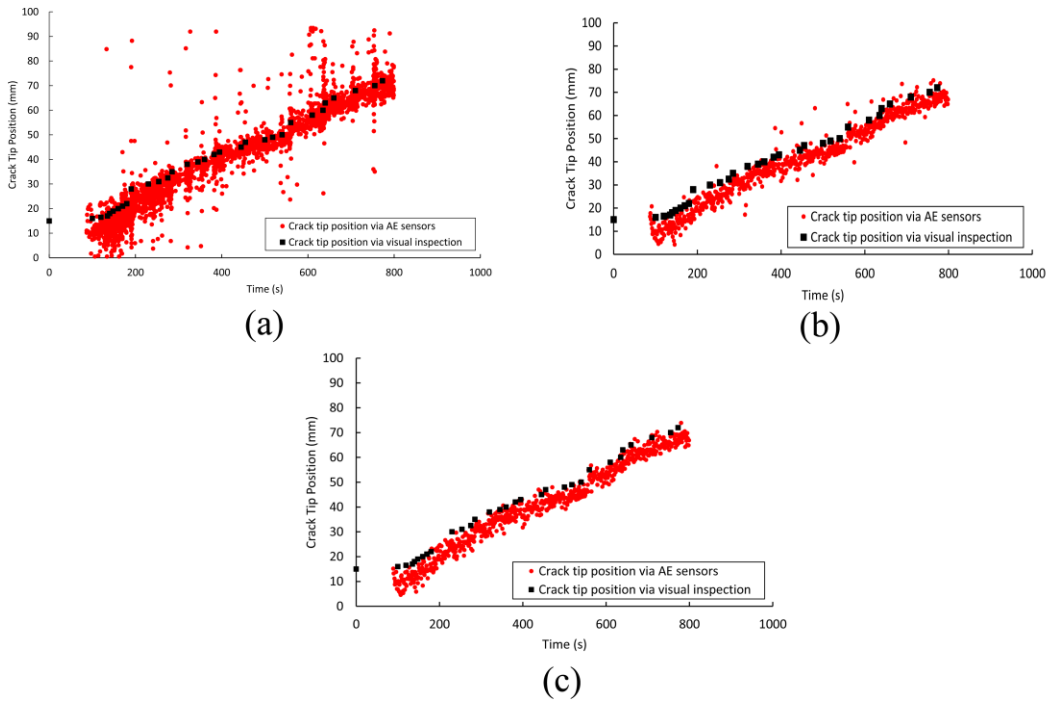


**Fig. 12** Crack tip position prediction using AE method

Table 3 shows the average and maximum differences between visual inspection based crack growth and AE based crack growth for the specimens.

**Table 3** Average and maximum differences of AE and visual based results

| Specimen | Average error (%) | Maximum error (%) |
|---|---|---|
| **U** | 3.5% | 8% |
| **W** | 4.4% | 10% |

In order to investigate performance accuracy of the method for different loading conditions, a similar specimen with specimen U ( U' ) is loaded by feed rate of 1 mm/min. Figure 13 shows the predicted crack tip position for specimen U'. Obtained results show good agreements between the visual inspection values and AE based crack tip position determination.

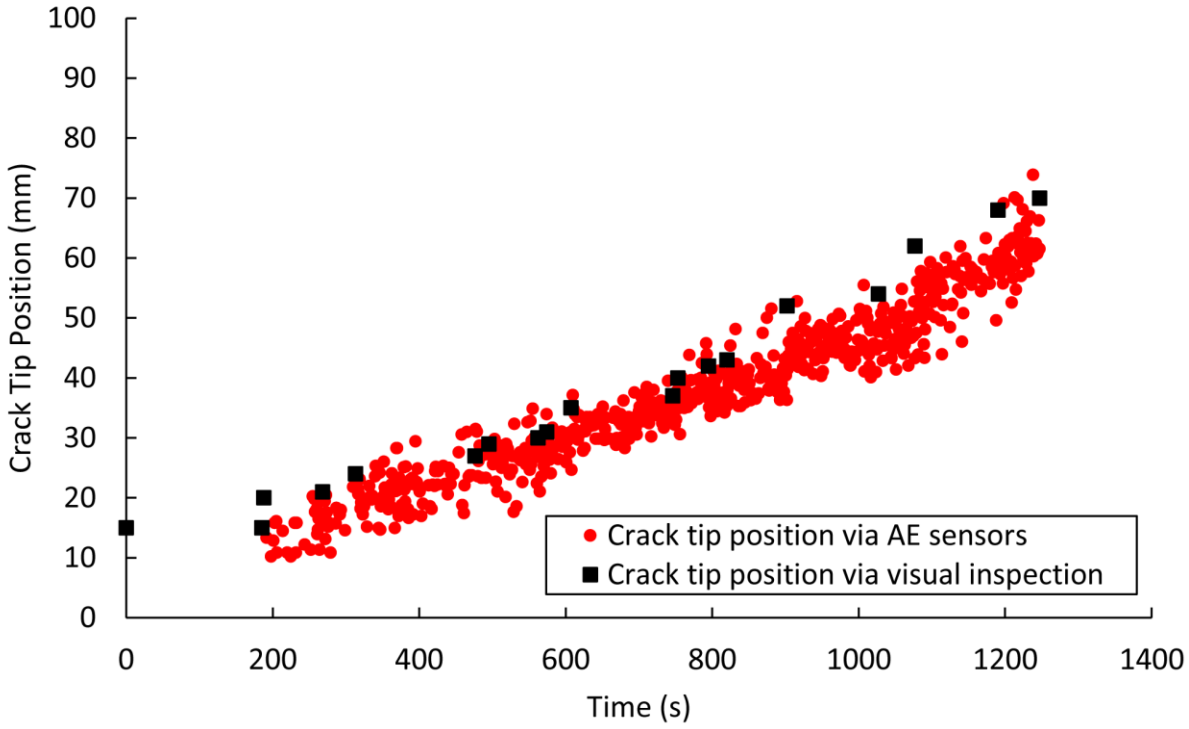


**Fig. 13** Predicted and actual crack tip position for specimen U'

A brief explanation of proposed crack tip position localization method is shown in Figure 14.

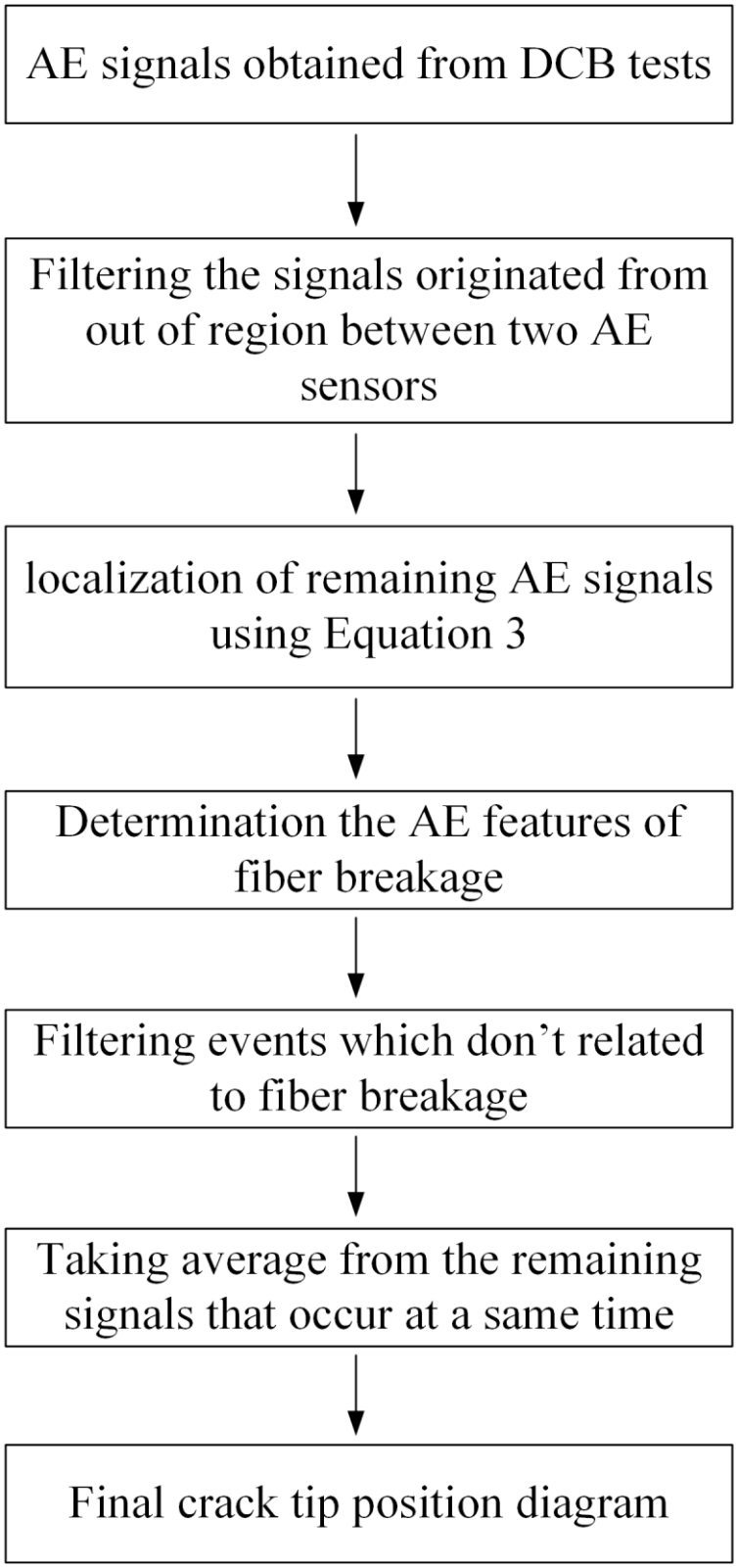


**Fig. 14** A brief explanation of proposed crack tip position localization method

### *3.2.2 Crack tip localization using cumulative AE energy*

Figure 14 shows load-displacement and cumulative energy-displacement diagrams for specimen U. According to Figures 14 and 4, crack growth and cumulative energy have a same trend and they have a linear relationship with displacement (time). Thus, according to Equation 4 crack growth can be related to the cumulative energy by a linear equation as follow:

$$\left.\begin{aligned}\Delta a &= A_1 \cdot d + A_2 \\ CE &= A_3 \cdot d + A_4\end{aligned}\right\} \Rightarrow \Delta a = A \cdot (CE) + B \qquad \text{(Eq. 4)}$$

Where A1, A2, A3, A4, A and B are the coefficient of the equations that are related to the material properties and loading conditions. $\Delta a$ is the crack growth and CE is the cumulative energy of the AE signals. Figure 15 shows linear relation between crack growth and cumulative energy for specimen U.

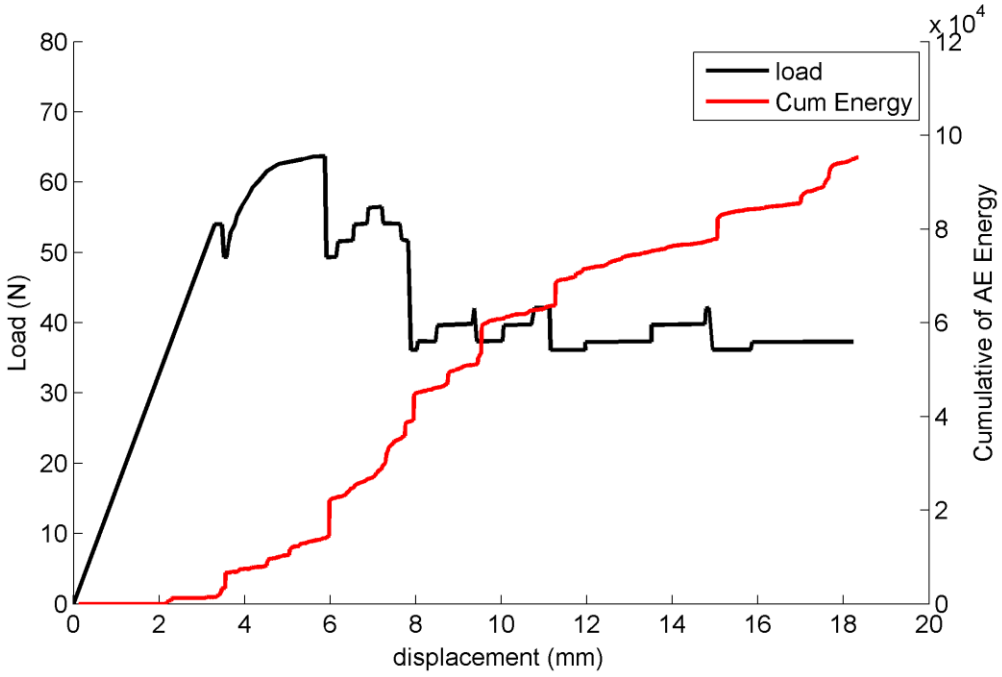


**Fig. 14** load-displacement and cumulative energy-displacement diagrams for specimen U

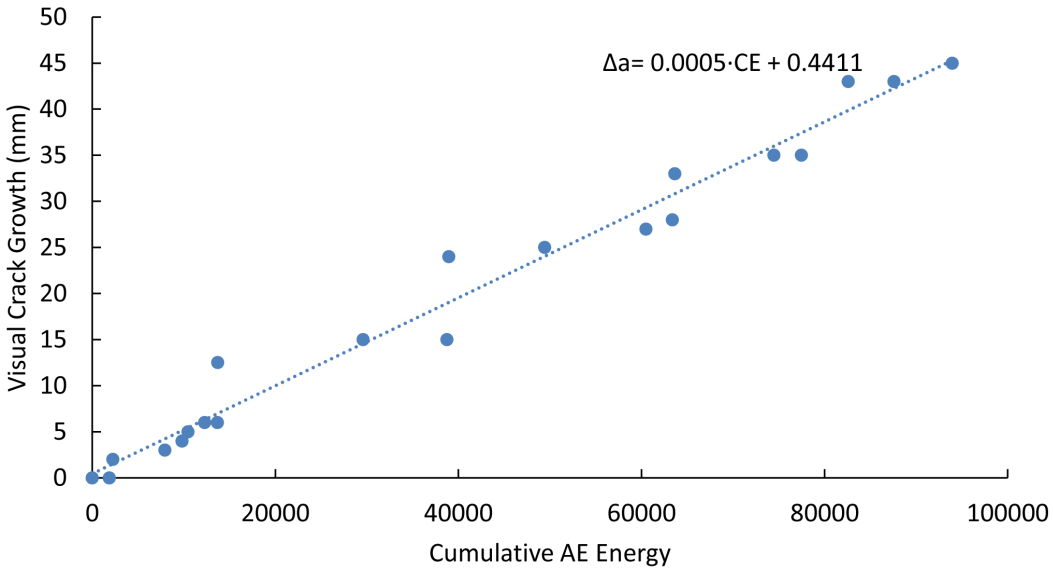


**Fig. 15** relation between crack growth and cumulative energy for specimen U

Figure 16 shows the predicted crack growth vs. visual crack growth curves for specimen U. As it can be seen, this method could predict crack growth very well.

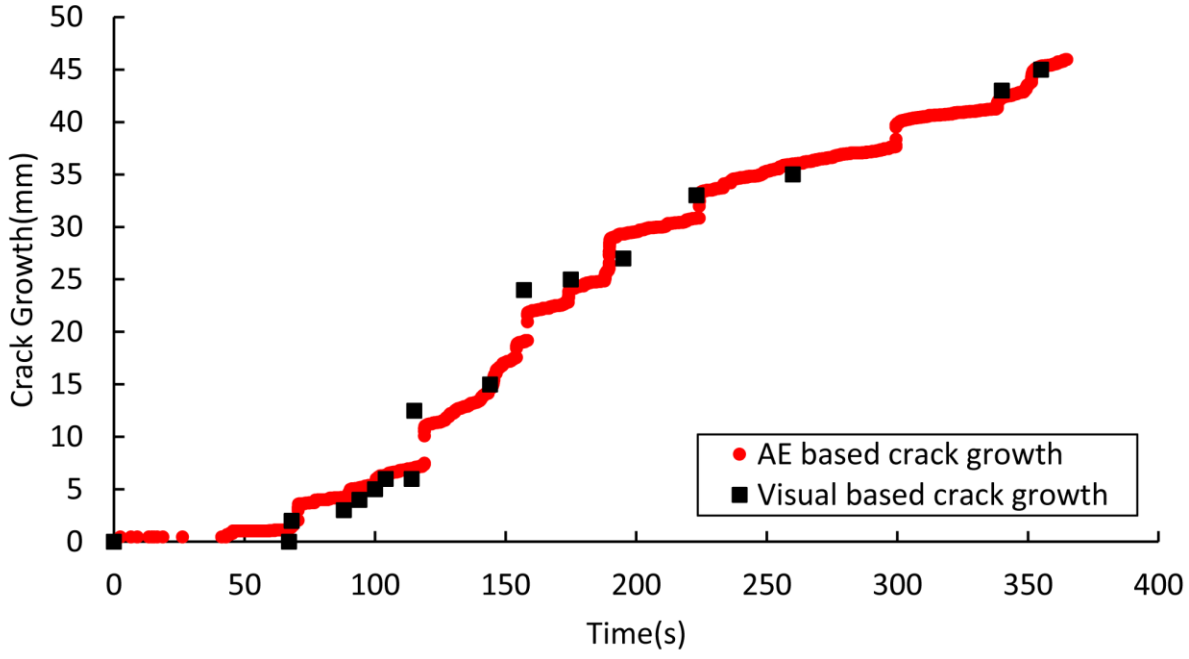


**Fig. 16** predicted crack growth vs. visual crack growth curves for specimen U

Figure 17.a shows the relation between crack growth and cumulative AE energy for specimen W. In order to investigate repeatability and reproducibility of coefficients for each test condition, the test is repeated (Figure 17.b). As it can be seen, the results have a good repeatability. As mentioned above, coefficient of the linear equation is a function of material properties and loading condition. Thus, the coefficient for specimen W is different from specimen U. In order to investigate loading effect on the coefficients of equation 4, similar specimen with specimen U ( $U^{'}$ ) was loaded by different feed rate. Specimen $U^{'}$ was loaded by feed rate of 1 mm/min. Coefficients of equation 4 for specimen $U^{'}$ is also shown in Figure 18. According to Figures 15 and 18, changing the loading condition changes the coefficient of equation 4 and therefore affects the predicted crack growth.

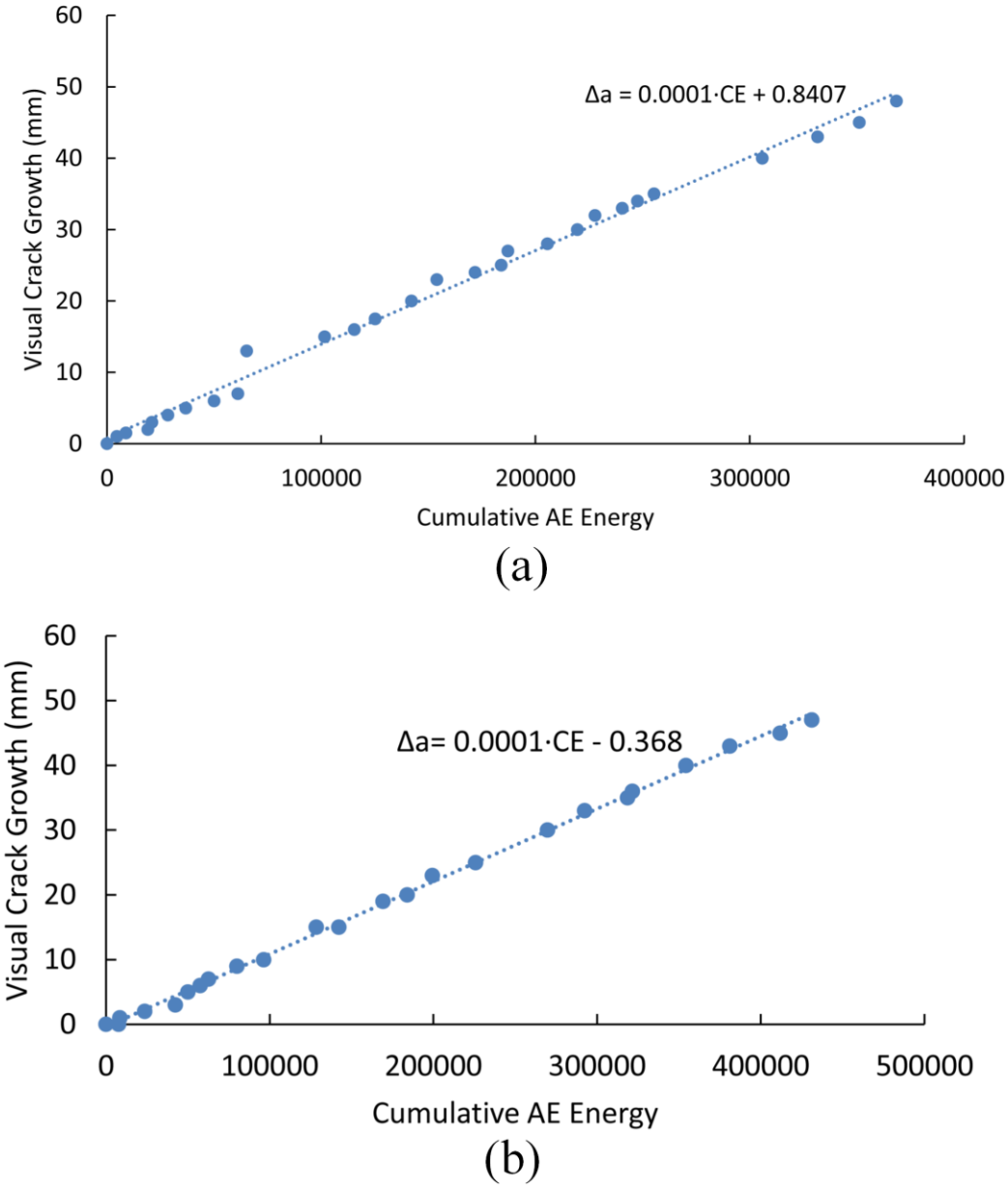


**Fig. 17** relation between crack growth and cumulative energy for specimen W and W'

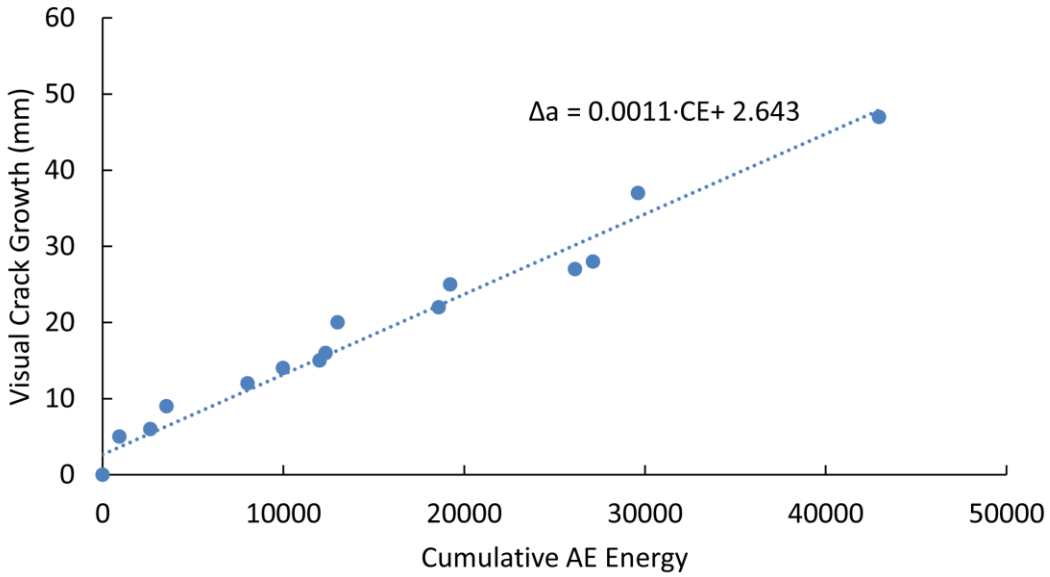


**Fig. 18** relation between crack growth and cumulative energy for specimen U'

Table 4 shows average and maximum errors of the results that obtained by the method for specimen U and W.

**Table 4**

| Specimens | Average error (%) | Maximum error (%) |
|---|---|---|
| **U** | 3.3% | 6% |
| **W** | 2.9% | 8% |

## *3.3 Critical strain energy measurement*

Based on the energy release rate failure criterion for mode I loading, crack growth begins when the available energy release rate, $G_I$, is equal to or greater than a critical value, $G_{IC}$. This quantity is considered to be a material characteristic that represents the interlaminar fracture toughness of the laminated composites. Accurate determination of $G_{IC}$ is an important issue that will help to better understand of the damage tolerances and durability analyses of laminated composites. In order to

evaluate $G_{IC}$ for laminated composite materials, some procedures presented in the ASTM D5528 standard []. In this section, in addition to the procedures that recommended by ASTM D5528, some new methods based on the AE information and the combination of mechanical and AE data are represented for evaluation $G_{IC}$. The proposed methods for evaluation of interlaminar fracture toughness are introduced below:

### *3.3.1 ASTM standards*

The $G_{IC}$ values are determined using the critical load and deflection ($P_C$ and $\delta_C$) measured: (a) at the point of deviation from linearity in the load–displacement curve (NL), (b) at the point at which delamination propagation is visually observed (VIS) and (c) at the point at which the compliance has increased by 5% or the load has reached a maximum value (5%/max). Figures 19 shows values of $P_C$ and $\delta_C$ which were obtained from the standard methods for specimens U and W.

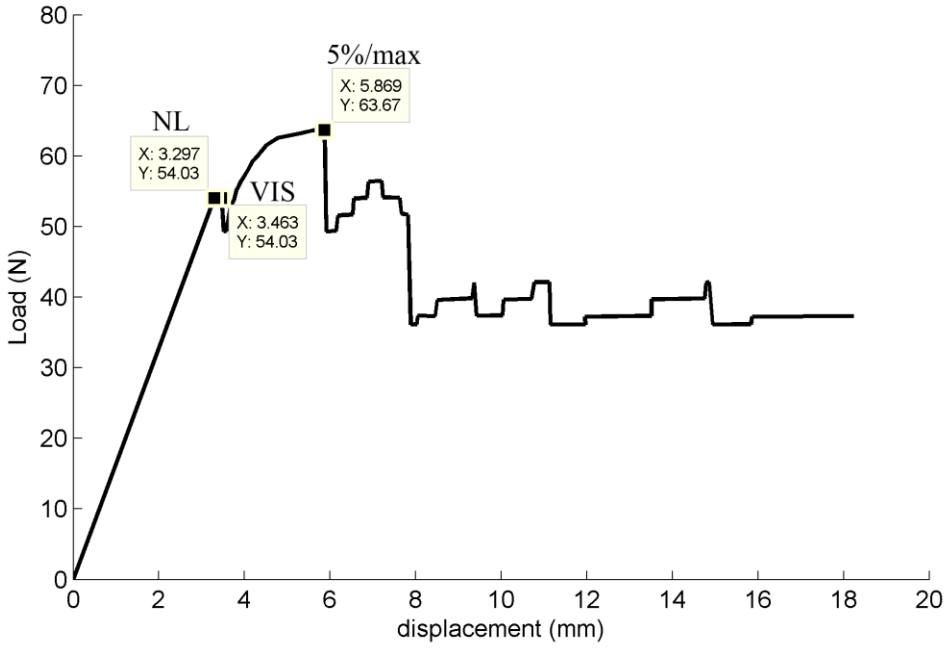

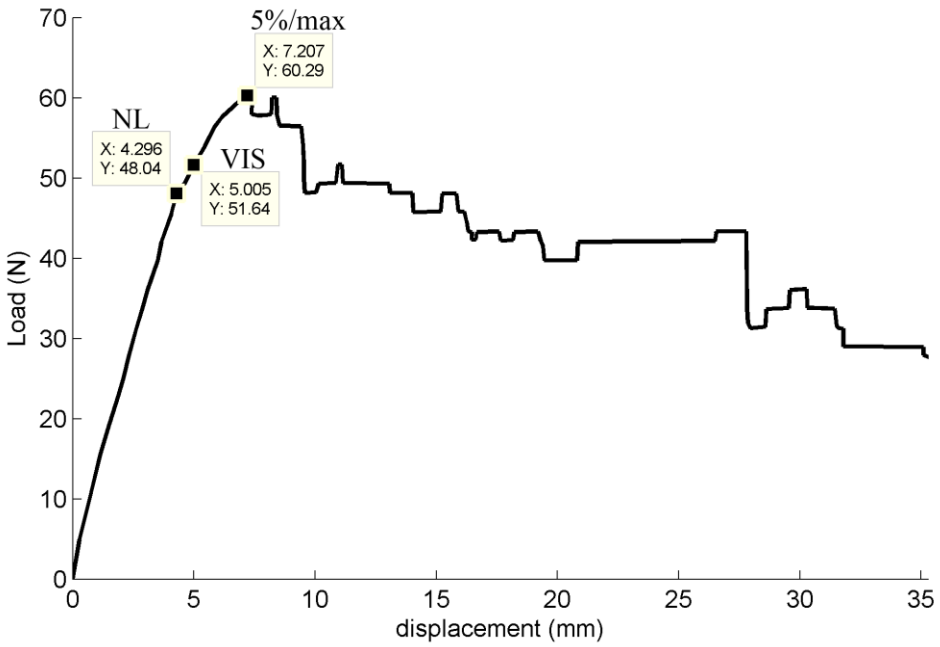


**Fig. 19** Critical load and displacement values ($P_C$ and $\delta_C$) obtained from ASTM standard methods for specimens U and W

Table 5 shows values of interlaminar fracture toughness of the specimens that obtained from the methods introduced in the ASTM D5528 standard.

**Table 5 The $G_C$ values obtained from ASTM standard methods for the specimens**

| **Specimens** | **$G_{IC}$ (kJ/m$^2$)** | | |
|---|---|---|---|
| | **NL** | **VIS** | **5%/max** |
| **U** | 0.240 | 0.252 | 0.503 |
| **W** | 0.290 | 0.363 | 0.611 |

### 3.3.2 *Acoustic Emission method*

According to the different region of the load-displacement curves of the specimens (Figure 3), AE behavior of the specimens can be divided to three regions (Figure 20). In region (a), because of no damage mechanisms occur in the specimen, thus no significant AE activity is observed. In region (b), by initiation of delamination the AE activities initiate instantaneously. In region (c), by activation of different damage mechanisms and growth of delamination in the specimens, more AE activities are observed.

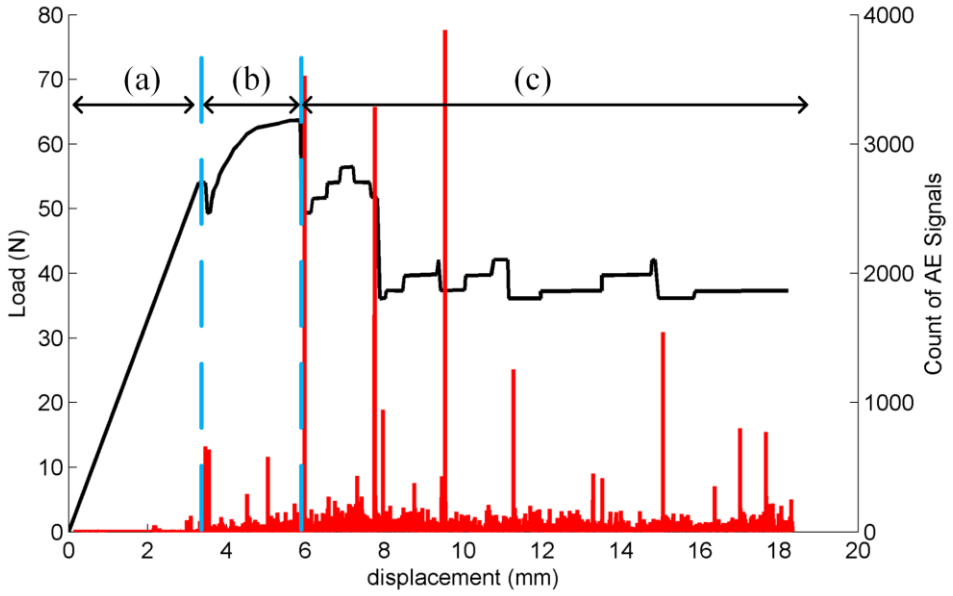


**Fig. 20**

In this section, the $G_{IC}$ values are determined using the critical load and deflection ($P_C$ and $\delta_C$) measured using different AE signal parameters: (a) at the point corresponding to the first sharp increase in the number of AE count and (b) at the point corresponding to the first sharp increase in the energy of AE signals. Figure 21 shows the values of $P_C$ and $\delta_C$ that obtained by these methods for specimen W. Table 6 represents the $G_{IC}$ values obtained by AE method for the specimens.

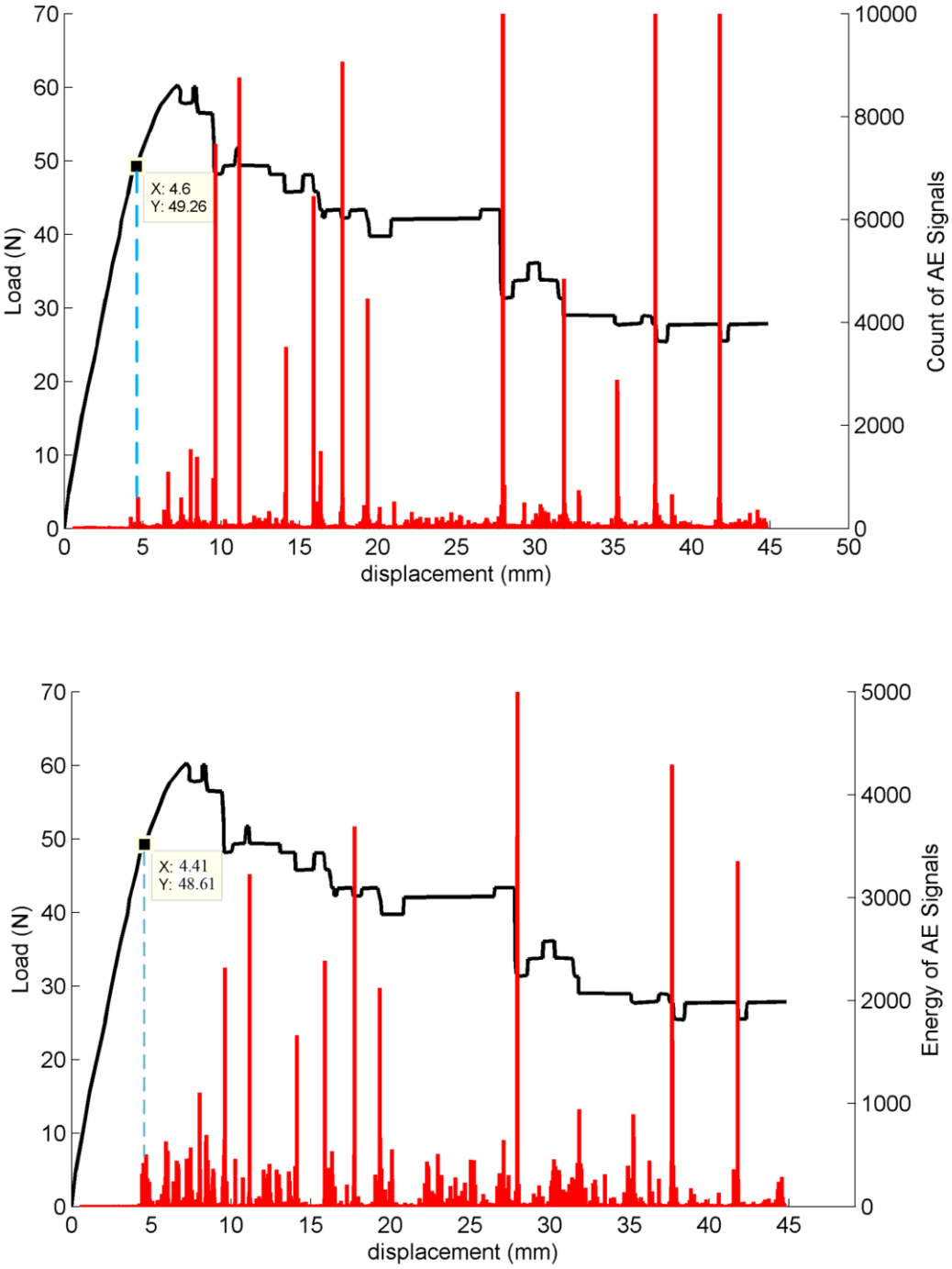


**Fig. 21** The energy of AE signals, during the initiation and propagation of the delamination in specimen U2

**Table 6** The $G_{IC}$ values obtained from the AE methods for the specimens

| Specimen | $G_{IC}$ (kJ/m$^2$) | |
|---|---|---|
| | $AE_{Count}$ | $AE_{Energy}$ |
| **U** | 0.252 | 0.241 |
| **W** | 0.318 | 0.301 |

### *3.3.3 Sentry function*

In the previous sections mechanical information and AE information were used separately for characterization of the damage. Combination of mechanical data and AE information could also be used to have comprehensive damage characterization in the specimens. The function which is used for this combination is called sentry function. As indicated by Eq 5, the sentry function is stated in the logarithm form of the ratio between mechanical and acoustical energies [18]:

$$f(x) = Ln\left[\frac{E_S(x)}{E_a(x)}\right] \qquad \text{(Eq.5)}$$

Where $E_S(x)$, $Ea(x)$ and $x$ are the strain energy, the AE events energy and the displacement, respectively. Sentry function is defined over displacement domain where the acoustic energy $Ea(x)$ is non zero. Depending on the material damaging process, the resulting f can assume any combination of the four trends. According to Figure 22, the parts of f characterized by an increasing trend, $P_I(x)$, represent the strain energy storing phases. When a significant internal material failure occurs, there is an instantaneous release of the stored energy that produces an AE event with high energy content. This fact is highlighted by the sudden drops of the function f that can be described by $P_{II}(x)$. The constant behavior of f, described by $P_{III}(x)$, is due to that rate of AE energy increases is equal to rate of strain energy storing in the specimens. The decreasing behavior of f, $P_{IV}(x)$, is related to the fact that the AE

activity is greater than the material strain energy storing capability, the damage has reached a maximum and the material has no resources to sustain the load. In order to determine $G_{IC}$, the first $P_{II}$ type of the sentry function is used to determine $P_C$ and $\delta_C$. Figure 22 shows the values of $P_C$ and $\delta_C$ that obtained by sentry function for the specimens. Table 7 represents values of $G_{IC}$ which were obtained by sentry function method for the specimens.

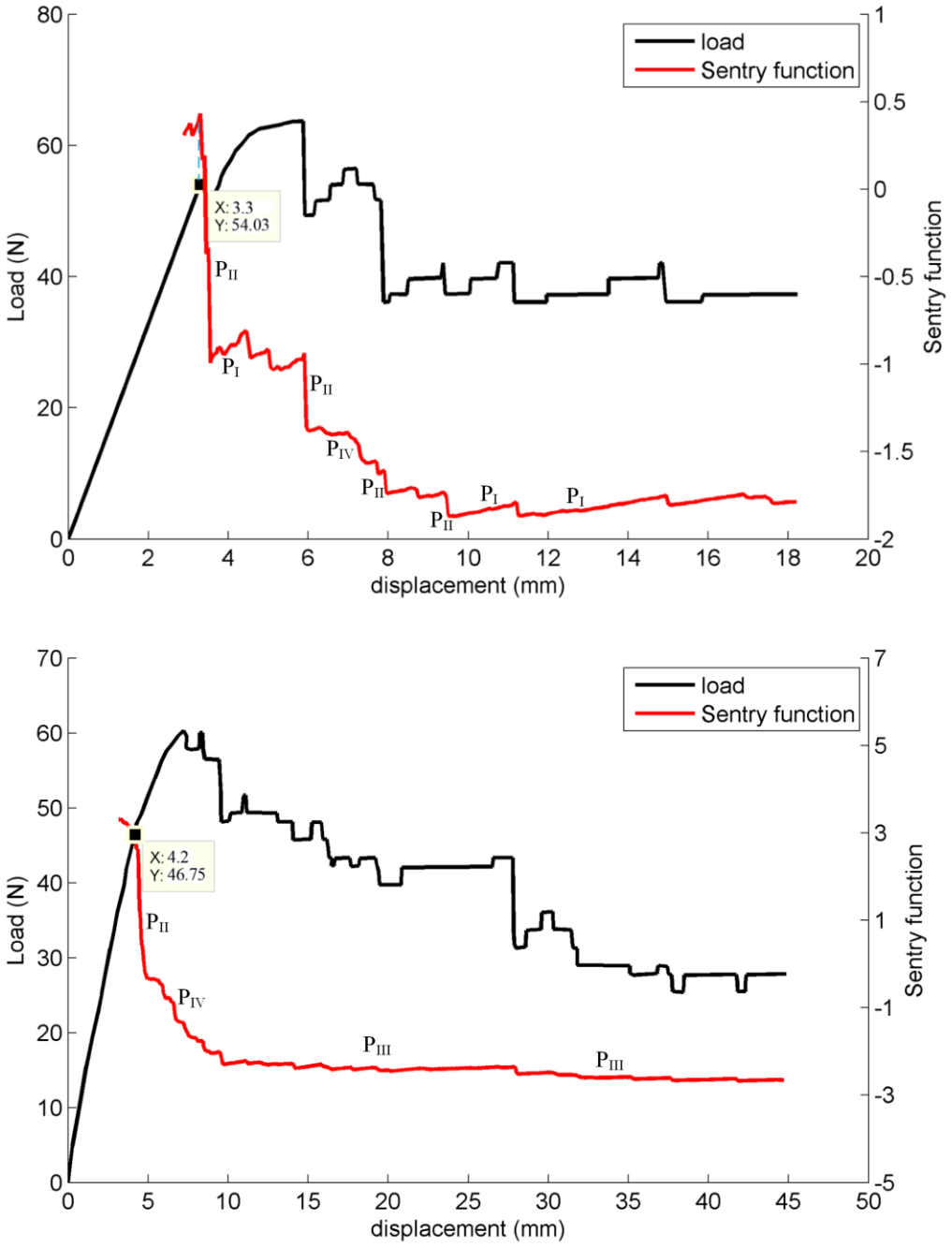


**Fig. 22** Determination of critical load value using sentry function approach, during the initiation and propagation of the delamination in the specimens

**Table 7** The $G_{IC}$ values obtained from the sentry function method for the specimens

| Specimen | $G_{IC}$ (kJ/m$^2$) |
|---|---|
| | **Sentry function** |
| **U** | 0.240 |
| **W** | 0.276 |

Table 8 and Figure 23 show values of interlaminar fracture toughness of the specimens which were obtained by the offered methods. As can be seen, through the methods that offered in the ASTM standards, NL method that recommended by ASTM standard gives the lower values compared to 5%/max and VIS methods [14]. Also, a large dispersion in the results obtained by standard methods is observed. The results obtained from AE and sentry function methods are most consistent with the results obtained from NL method. Because of the sentry function related to mechanical and AE events in the specimens, it has additional sensitivity to the occurrence of damages in the specimens. Thus, the sentry function gives the lower bound of the $G_C$ values. The AE and sentry function results dispersion are less than standard results. Because of dependency of VIS method to the operator skill, this method has low repeatability and gives upper bound of the $G_C$ values. VIS method, because of occurs quite likely later than initiation of delamination, Inter-laboratory variations, operator-dependent variations and dependency on delamination behavior (stable or un-stable) are some weak points of the previous standard methods. Also, due to different layup of the specimens, values of the $G_{IC}$ in the specimens are different.

**Table 8 Comparison $G_C$ values obtained from the offered methods for the specimens**

| Specimen | $G_{IC}$ (kJ/m$^2$) | | | | | |
|---|---|---|---|---|---|---|
| | ASTM (NL) | ASTM (VIS) | ASTM (5%/max) | $AE_{Count}$ | $AE_{Energy}$ | Sentry |
| U | 0.240 | 0.252 | 0.503 | 0.252 | 0.241 | 0.240 |
| W | 0.290 | 0.363 | 0.611 | 0.318 | 0.301 | 0.276 |

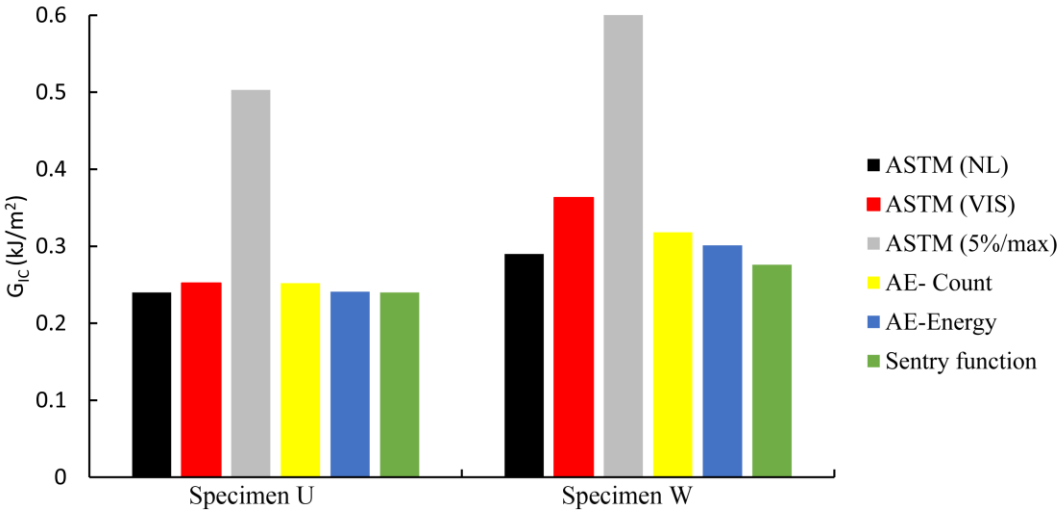


**Fig. 23** The values of the $G_C$ for the specimens which were obtained from the offered methods

# 4. Conclusion

In this paper, the relationship between AE absolute energy rate and stress intensity range is first described. A theoretical model for relating AE absolute energy rate to crack growth rate is subsequently developed for fatigue life prediction. The AE fatigue damage evaluation and fatigue life

prediction procedures may be simplified because the model is independent of stress intensity range. Passive piezoelectric sensing and conventional fatigue tests are carried out to detect AE and crack growth behavior using specially designed and fabricated compact tension (CT) specimens made of ASTM A572G50. Extraneous sources of noise in the AE dataset are filtered through a combined approach involving Swansong II Filters and investigation of waveforms, which are appropriate for data filtering and interpretation of field tests. The critical level of crack growth is determined by associating cumulative AE absolute energy and counts with crack length. Based on the experimental results and presented model, procedures for predicting crack extension and remaining fatigue life are demonstrated. The presented model and procedures are verified by comparing the predicted cracks with experimental data. The AE absolute energy rate curve is compared with the AE count rate curve. This study is limited to Mode I fatigue cracks. The resulting dataset is interpreted using the principles of linear elastic fracture mechanics (LEFM).

AE technique has high sensitivity and demonstrated reliability in detection of active cracks [6, 7], and can provide insight to the integrity of in-service composite structures and components [8–11]. Another notable advantage of the AE technique is the capability of locating active cracks in the region where a crack is likely to occur. Detecting cracking signals is a necessary step in the application of AE techniques. In addition to cracking signals, AE sensors are also sensitive to environmental noises. In this study, in order to discriminate hit and noise signals some hardware and software filtration methods were used [15–17]. Waveform features such as rise time, duration and amplitude were involved in filtering of the AE data [18–20]. [21, 22][Jianguo Yu, Paul Ziehl].

In addition, ASTM introduced methods for evaluation of mode I critical strain energy has some weaknesses in the case of repeatability and accuracy.

1. S. Sridharan, Delamination Behaviour of Composites, *CRC Press*, New York, 2008.
2. S. Benmedakhene, M. Kenane, and M. L. Benzeggagh, Initiation and growth of delamination in glass/epoxy composites subjected to static and dynamic loading by acoustic emission monitoring, *Compos. Sci. Technol.*, 1999, vol.59, pp. 201-208.
3. A.A. Bakhtiary Davijani, M. Hajikhani, M. Ahmadi, Acoustic Emission based on sentry function to monitor the initiation of delamination in composite materials, *Mater. Des.*, 2011, 32: 3059–3065.
4. A.B. de Morais, A.B. Pereira, M.F.S.F. de Moura, A.G. Magalhães, Mode III interlaminar fracture of carbon/epoxy laminates using the edge crack torsion (ECT) test, *Compos. Sci. Technol.,* Volume 69, 2009, Issue 5, Pages 670–676.
5. A. Refahi Oskouei, A. Zucchelli, M. Ahmadi and G. Minak, An integrated approach based on acoustic emission and mechanical information to evaluate the delamination fracture toughness at mode I in composite laminate, *Mater. Des.*, 2011, 32(3):1444–1455.
6. M. Fotouhi, H. Heidary, M. Ahmadi and F. Pashmforoush, Characterization of composite materials damage under quasi-static three-point bending test using wavelet and fuzzy C-means clustering, *J. Compos. Mater.*, 2012, 46(15):1795-1808.
7. S. Huguet, N. Godin, R. Gaertner, L. Salmon and D. Villard, Use of acoustic emission to identify damage modes in glass fibre reinforced polyester, *Compos. Sci. Technol.*, 2002, 62(10–11):1433–44.
8. F. Pashmforoush, M. Fotouhi and M. Ahmadi, Acoustic emission-based damage classification of glass/polyester composites using harmony search k-means algorithm, J. Reinf. Plast. Compos., 2012, 31: 671-680.
9. T.L. Anderson, Fracture Mechanics; fundamentals and applications, *Taylor & Francis*, 2005.
10. Aggelis D.G., Kordatos E.Z., Matikas T.E., Acoustic emission for fatigue damage characterization in metal plates, Mechanics Research Communications, 2011. 38(2): p. 106-110.
11. Ai Q., Liu C., Chen X., He P., Wang Y., Acoustic emission of fatigue crack in pressure pipe under cyclic pressure, Nuclear Engineering and Design, 2010. 240(10): p. 3616-3620.
12. Rabiei M., Modarres M., Quantitative methods for structural health management using in situ acoustic emission monitoring, International Journal of Fatigue, 2013. 49: p. 81-89.
13. Babu, M.N., Mukhopadhyay C. K., Sasikala G., Dutt B., Shashank S., Albert S. Bhaduri A. K., Jayakumar T., Fatigue Crack Growth Characterisation of RAFM Steel using Acoustic Emission Technique, Procedia Engineering, 2013. 55: p. 722-726.
14. Roberts T.M., Talebzadeh M., Acoustic emission monitoring of fatigue crack propagation, Journal of Constructional Steel Research, 2003. 59(6):p. 695-712.

15. Roberts T.M., Talebzadeh M., Fatigue life prediction based on crack propagation and acoustic emission count rates, Journal of Constructional Steel Research, 2003. 59(6): p. 679-694.
16. Yu J., Ziehl P., Zárate B., Caicedo J., Prediction of fatigue crack growth in steel bridge components using acoustic emission, Journal of Constructional Steel Research, 2011. 67(8): p. 1254-1260.
17. Yu J., Ziehl P., Stable and unstable fatigue prediction for A572 structural steel using acoustic emission, Journal of Constructional Steel Research, 2012. 77: p. 173-179.
18. Romhany G., Szebényi G., Interlaminar fatigue crack growth behavior of MWCNT/carbon fiber reinforced hybrid composites monitored via newly developed acoustic emission method, Express Polymer Letters, 2012. 6(7): p. 572-580.
19. Paget C.A., Delamination Location and Size by Modified Acoustic Emission on Cross-ply CFRP Laminates during Compression-Compression Fatigue Loading,ICCM17proceedings. 2009: UK.
20. Refahi Oskouei A., Ahmadi M., Acoustic Emission Characteristics of Mode I Delamination in Glass/Polyester Composites, Journal of Composite Materials, 2010. 44(7): p. 793-807.
21. Arumugam V., Suresh Kumar C., Santulli C., Sarasini F., Joseph Stanley A., A Global Method for the Identification of Failure Modes in Fiberglass Using Acoustic Emission, Journal of Testing and Evaluation, 2011. 39(5).
22. Silversides I., Maslouhi A., LaPlante G., Interlaminar fracture characterization in composite materials by using acoustic emission, 5th International Symposium on NDT in Aerospace. 2013: Singapore.
23. ASTM D5528-01, Standard Test Method for Mode I Interlaminar Fracture Toughness of Unidirectional Fiber-Reinforced Polymer Matrix Composites. 2007, ASTM International: West Conshohocken, PA.
24. Anderson T.L., FRACTURE MECHANICS; Fundamentals and Applications, Third ed. 2005: Taylor & Francis Group.
25. Silversides, I. Maslouhi, A. LaPlante, G., Acoustic emission monitoring of interlaminar delamination onset in carbon fibre composites, Structural Health Monitoring, 2013, DOI: 10.1177/1475921712469994.
26. M.L. Benzeggagh, M. Kenane, Measurement of mixed-mode delamination fracture toughness of unidirectional glass/epoxy composites with mixed-mode bending apparatus, Composites Science and Technology, Volume 56, Issue 4, 1996, Pages 439–449.
27. M. Kenane, M.L. Benzeggagh, Mixed-mode delamination fracture toughness of unidirectional glass/epoxy composites under fatigue loading, Composites Science and Technology, Volume 57, Issue 5, 1997, Pages 597–605.

28. Jie Xu, Qinghua Han, Giuseppe Lacidogna, Alberto Carpinteri, Accuracy of Acoustic Emission Localization for Masonry Structures Monitoring, 13th International Conference on Fracture, 2013, Beijing, China
29. Liying Sun, Yibo Li, Acoustic emission sound source localization for crack in the pipeline Control and Decision Conference (CCDC), 2010 Chinese